URSI GASS 2021, Rome, Italy, 28 August - 4 September 2021

Optimizing Radiofrequency Field and Induction Coupling in Slotted Cold Crucibles

Marco Cavenago*[(1)], Michele Comunian[(1)], Giorgio Keppel[(1)], Antonio Rossi[(2)] and Francesco Sciarrabba[(1)]
(1) INFN-LNL, viale dell'Universitá n.2 , 35020 Legnaro (PD) Italy, http://www.lnl.infn.it
(2) Officina dei Materiali, Romano d'Ezzelino (VI), Italy

Abstract

Using radiofrequency (rf) for heating and levitation of alloy samples is greatly simplified by a passive element, the slotted cold crucible (similar to Faraday shield for rf plasma ion sources), which if properly designed can shape and concentrate the axial (non static) magnetic field profile. The effect is better represented and verified in 3D simulations (very time consuming) as shown here, even if some simplified 1D and 2D models may help understanding. Boundary conditions at large radius are discussed. Moreover, the sensitivity to important parameters (levitated weight vs frequency and power, sizes of crucible, sample conductivity, radius of sample to skin depth ratio) are demonstrated in a schematized 3D geometry, easily parametrized. Finally complete 3D simulation of a realistic design (adequate for clean alloy melting) are also reported.

1 Introduction

Radiofrequency heating is well established in several application, including ion source plasma[1], so that its use for melting alloys (or heating samples) is natural[2]; the Lorentz force on current induced in the sample may (on average) support the sample against gravity, providing levitation for adequate objects and magnetic field **B** profiles; let us consider cylindrical coordinates $Or\psi z$, with gravity directed towards the negative z. For simplicity let sample be a radius R_s sphere (or an ellipsoid, see Fig. 1), centered at z_s; all coils have the same axis z and one only angular frequency ω, with frequency $f = \omega/2\pi$ ranging from 1 kHz to 10 MHz as later optimized. Since induced current is mostly in ψ direction, the support force has a zero on the z axis, where sample is supported by surface tension and dynamical effects[2], to be verified in following studies; here we simply compute the total rf power P_t and the total force F_z for a given total sample volume V_s, defining the average critical density:

$$d_a = F_z/(gV_s) \quad , \quad d_w = d_a/P_t \tag{1}$$

to be compared with d_s the density of sample; of course $d_s < d_a$ is a necessary (but not sufficient) condition for levitation, otherwise the sample will fall; in other words, when the critical density per unit power d_w is calculated, we know that $P_t > d_s/d_w$ for levitation. We have vector potential $\mathbf{A} \cong \Re\, \hat{\psi} A_\psi(r,z)\mathrm{e}^{\mathrm{i}\omega t}$; the real part $\Re$ operator is usually

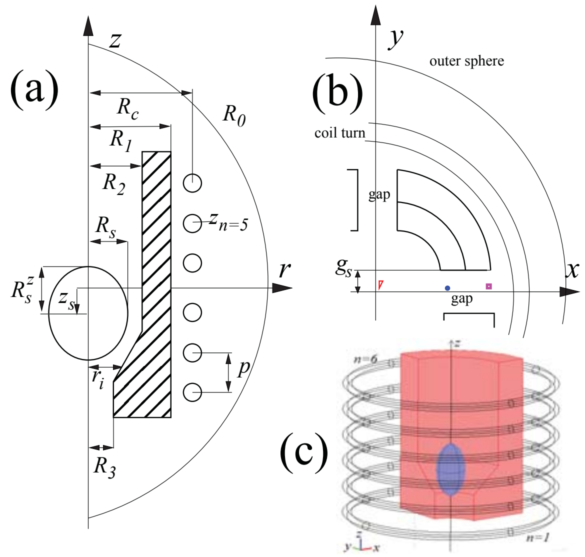

Figure 1. Sketch of test geometry (not to scale): (a) rz section (note size definitions); (b) quarter of xy section (sample omitted); (c) 3D view of coil, sample and a quarter of crucible.

omitted (phasor notation). The rf power is dissipated in the coil, in the crucible (with conductivity σ_c) and in the sample (with conductivity σ_s), mainly dependent from their skin depths

$$\delta_s = (\mu\omega\sigma_s/2)^{-1/2} \quad , \quad \delta_c = (\mu\omega\sigma_c/2)^{-1/2} \tag{2}$$

When $\delta_s \ll R_s$ the power loss in sample P_s is easily estimated by a surface integral

$$P_s = \frac{1}{2}\int \mathrm{d}S Z_s^r |\mathbf{H}_\parallel|^2 \quad , \quad Z_s = (1+\mathrm{i})/\sigma_s\delta_s = (\mathrm{i}\mu\omega/\sigma_s)^{1/2} \tag{3}$$

where $Z_s^r = \Re Z_s$ with Z_s the planar surface impedance, dS is the surface element and $\mathbf{H}_\parallel$ are the tangential components of the magnetic field. Similarly for coils and crucible, with impedance Z_c, which is convenient to keep as low as economically feasible; this implies they are made of copper alloys (with water cooled channels); we define the parameter $M = R_s/\delta_s$, so eq. 3 applies for large M. For any M, in 3D simulations, power loss P_t is calculated from applied voltage and currents and also verified by volume integrals.

2 The 3D test simulation setup

As shown in Fig. 1, the helical coil of pitch p with N complete turns can be approximated with N rings with conductor radius R_w, average coil radius R_c, provided that[3] each ring has an infinitesimal thin cut to apply a voltage V_n[3] per turn for current control; due to crucible $\phi \cong 0$ except for coil applied voltage. Since $\mathbf{E} = -\mathbf{A}_{,t} - \nabla\phi$, the total current density results

$$\mathbf{j} = \sigma\mathbf{E} = -\sigma[\mathrm{i}\omega\mathbf{A} + (2\pi r)^{-1}V_n] \tag{4}$$

The current I_n in each ring n must equal one common value I_c, so that V_n must be adjusted until $I_n = I_c$ (most solvers[5] now include this option; otherwise, V_n is iteratively adjusted by an user code until $I_n = I_c$ is satisfied within 0.02% tolerance). The Maxwell equation

$$\nabla\times\mathbf{H} = \mathbf{j} + \mathbf{D}_{,t} \quad , \quad \mathbf{H} = \mu^{-1}\nabla\times\mathbf{A} \tag{5}$$

is discretized using so-called edge elements[4] for $\mathbf{A}$ (complicate details about gauge fixing and differentiation of $\mathbf{A}$ are discussed elsewhere [5]). Note that $\mathbf{D}_{,t}$ is of order $(\omega R_c/c)^2$ and thus usually negligible. At material interfaces, we have the conditions of continuity of $H_\parallel$ and of normal component B_n of the magnetic flux density.

To complete geometry description, the ring assembly height is $L_a = (N-1)p + 2R_w$ (the real helical coil length is $Np + 2R_w$), while shortest distance between rings is $p - 2R_w$; in our test case, $N = 6$, $p = 0.02$ m and $R_c = 0.07$ m, so that L_a and $2R_c$ are comparable. Crucible outer radius is $R_1 = 0.06$, length $L_c = 0.12$ m, while inner radius ranges from $R_3 = 0.02$ (lower hole) to $R_2 = 0.04$ m (upper hole); gap semiwidth g_s is 1 mm. We define a cartesian system $Oxyz$ and spherical system $O\rho\theta\psi$ related to cylindrical $Or\psi z$ by $\rho^2 = r^2 + z^2 = x^2 + y^2 + z^2$ and $z = \rho\cos\theta$ (please note θ is the polar angle while ψ is the azimuth and ρ the spherical radius). Outer boundary is a large spherical surface $\rho = R_0$; in our example $R_0 = 0.31$ m.

It is convenient to simulate only one quarter of geometry, using symmetry at planes xz and yz; here the boundary condition (bc) is $B_n = 0$, that is no field line crosses these surfaces, that is magnetic insulation (for connected boundaries this gives $\mathbf{A}_\parallel = 0$). As to the outer sphere, even for reasonably large R_0, magnetic insulation is a fair to poor approximation; the seemingly simpler $H_\parallel = 0$ (negligible magnetic field) condition is also worst; multiphysics codes now offer the option to add infinite elements around the R_0 sphere, at the price of computation time. Alternatively, a physically correct boundary condition is the dipole one, see eq. 7, as shown just below. Note that for large ρ the quadrupole and higher terms are negligible respect to the dipole term

$$A_\psi = -\frac{\mu_0 m_d}{4\pi}\frac{\sin\theta}{\rho^2}(1 - \mathrm{i}k\rho)\mathrm{e}^{\mathrm{i}k\rho} \tag{6}$$

with $k = \omega/c$ and $m_d \equiv \frac{1}{2}\int \mathbf{x}\times\mathbf{j}\,\mathrm{d}^3x$, with d^3x the volume element; the dipole term satisfies the bc:

$$-\mathbf{n}\times\mathbf{H} = \frac{k_c}{\mu_0 R_0}\mathscr{P}\mathbf{A} \quad , \quad \mathscr{P} = \frac{1}{r^2}\begin{bmatrix} -y^2 & xy & 0 \\ xy & -x^2 & 0 \\ 0 & 0 & 0 \end{bmatrix} \tag{7}$$

and $k_c \cong (1 - \frac{1}{2}k_0^2)/(1 + \frac{1}{2}k_0^2)$ with $k_0 = \omega R_0/c$, as verified by standard calculations. For no crucible case, the dipole moment is $m_d = \pi N R_c^2 I_c$. Otherwise, let $z = z_n$ the middle plane of each ring and C_n the area of the crucible cut by this plane; in first approximation, the dipole moment m_n (due to n-th ring) is reduced as the ratio of this area to whole ring enclosed area πR_c^2. Thus $m_n = \pi R_c^2 I_c E_n$ with factor $E_n = 1 - (C_n/\pi R_c^2)$ related the empty space fraction inside ring and $m_d = \sum_n m_n$. Moreover the weighted average of ring positions $z_c = \sum z_n m_n/m_d$ is computed before simulation, and coil, crucible, and load are translated by $-z_c$. After translation $z_c = 0$; this coil centering further suppresses non-dipole terms, as verified at simulation end, by a plot of $\mathbf{H}_\parallel$ on the outer sphere.

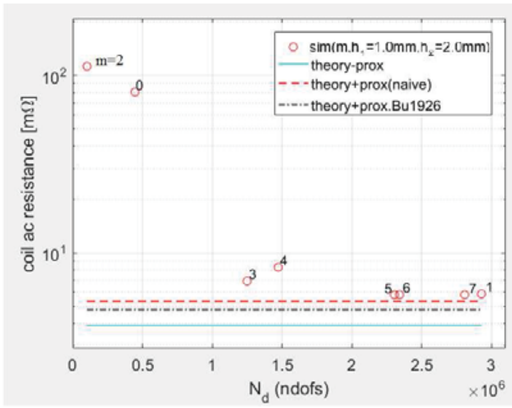

Figure 2. Simulated resistance of a pure coil vs. N_d (ndof), for several mesh styles $m = 0,\ldots,7$, as labeled, with parameters h_1, h_2 (see text for their definition); theory results without ('-prox') and with proximity ('+prox') effect are shown as lines; Bu1926 is Ref[6].

3 Simulation validation and results

Making a 3D model mesh requests several choices of where to refine the mesh, which should be thinner than δ_c at crucible and coil faces; several mesh styles (numbered with m in Fig. 2) were compared at $f = 400$ kHz, perhaps with local refinements h_1 (coil surface element size) and h_2 (element size of some crucible surface) added to solver standards. The solver normal mesh is $m = 2$ (actually very coarse), the finest standard solver mesh is $m = 1$, while $m = 0$ refines normal mesh only on gap surface; other cases add more local refinements to a moderately fine mesh; finally style $m = 7$ uses layer elements thinner than δ in the coil and the sample. The impedance $Z_c(coil)$ of an rf coil is well-known[6, 7], even if several effect needs to be taken into account, including skin depth and proximity effects. Simulations, when crucible and load conductivities are set to zero, must match result: let $Z_c(sim) = \sum V_n/I_c$. The resis-

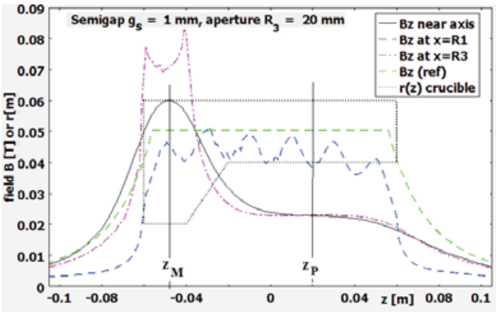

Figure 3. The near axis field $B_z(0,0,z)$ (solid line) with maximum at z_M and plateau at z_P; note also: the crucible outline (dotted line), the field B_z for $x = R_1$ and $y \ll g_s$ (dashed line), where the six coil turn peaks are visible, and for $x = R_1$ and $y \ll g_s$ (dot-dashed line), where compression at z_M and corner peaks are visible.

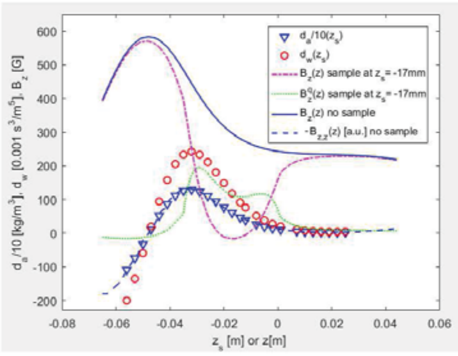

Figure 4. Comparison of fields with and without a $\sigma_s = 10^6$ S/m sample for $f = 21$ kHz; also the lift d_a and d_w are shown for several z_s (sample center); see text for B_z^q

tive part is shown in Fig. 2; by increasing the number of degrees of freedom (ndof) N_d the value $\Re Z_c(sim)$ approaches $\Re Z_c(coil)$ very much, still leaving some error (maybe due to theoretical estimate). The reactive part is larger, so relative errors respect to the well-known Nagaoka formula[7] are negligible (less than 1%). The meshes are kept unchanged during solution and scans, and style $m = 7$ was finally chosen. With direct solver, $N_d = 3 \times 10^6$ dofs requires 100 GB RAM, a practical limit especially for scans.

Crucible and coil conductivity were set to $\sigma_c = 5.8 \times 10^7$ S/m (cooled copper, plumbing grade) in fig. 3, showing B_z on axis for $I_c = $ i800 A and σ_s negligible; note the strong asymmetry induced by crucible shaping in an otherwise symmetric coil (no taper); ratio $\mathscr{R}(z_M, z_P)$ of $B_z|_{axis}$ at z_M and z_P is satisfactorily about 2.5, which increases to 3 when B_z on the line $y = 0$ and $x = R_3$ is considered. Indeed the flux $\Phi^i(z) \cong \pi B_z r_i^2$ inside crucible inner radius $r_i(z)$ would be constant if $N_c g_s = 0$ with N_c the number of cuts; more precisely, the flux change (leak or increase) rate is

$$\Phi^i_{,z} = -2 N_c g_s B_x(r_i^+, 0, z) \quad , \quad r_i^+ = r_i + \varepsilon_i \qquad (8)$$

which is part of an approximate 1D model for Φ^i and B_x; here ε_i is a small positive length, say $\varepsilon_i \cong g_s$. This

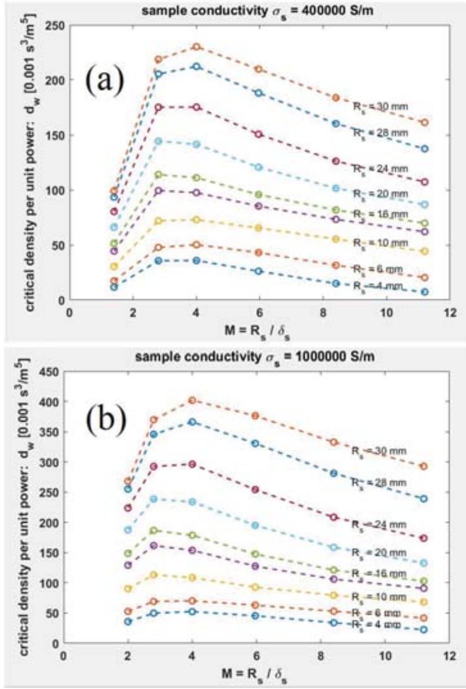

Figure 5. The critical density per unit power d_w for several sample radii vs merit factor M; (a) a lower conductivity case; (b) higher σ_s

model will give $\mathscr{R}(z_M, z_P) \cong (r_i(z_P)/r_i(z_M))^\alpha \cong 4$ with $\alpha = 2 + O(N_c g_s/R_3)$; from fig. 4 data we see $\alpha \cong 1.3$ for flux leakage. The actual $\mathscr{L}_c \equiv N_c g_s/R_2 = 0.1$ (named leakage parameter, necessarily $\mathscr{L}_c < \pi$) here shown is a compromise between trapping flux in the crucible taper and accumulating flux in the $r_i = R_2$ part. In Fig. 3, note also the naive estimate $B_z^{ref} = \mu_0 I_c/p$ and the field on the $x = R_1$ line [at square marker in Fig. 1.(b)], which shows oscillation due to coil structure and an average lower than B_z^{ref} by a factor similar to f_N, the well-known Nagaoka factor f_N [7], roughly $f_N \cong 1/(1 + 0.9R_c/(Np))$.

Reported conductivity is about $\sigma_s = 6 \times 10^5$ S/m for Ti just above melting point (or 10^6 S/m for liquid Mo), then it decreases with temperature[8], so range $\sigma_s = [0.4, 1] \times 10^6$ S/m is studied here. A $\sigma_s > 0$ modifies the $B_z(z)$ profile, making a valley around z_s as shown in fig. 4; moreover the field phase changes significantly in the sample, as shown by B_z^q (component in quadrature wrt I_c). Anyway $d_a(z_s)$ as a function of z_s seems closely proportional to $-B_{z,zz}(z)$ from fig. 3 data, (no sample) at least for the simulated condition ($f = 21$ kHz, with a an ellipsoidal sample, xy section radius $R_s = 0.01$ m, semi-height 0.02 m), which is remarkable. Since f is constant, also d_w is roughly proportional to fig. 3 result for $-B_{z,z}$. For stability, the lift must decrease when z_s increases, which give the criterion $B_{z,zz}(z_s) < 0$, satisfactorily satisfied in a large interval (including taper of r_i); for adequate power, an equilibrium z_s is then possible. Finally in Fig. 5, with $z_s = -17$ mm fixed, effect of R_s change and ω change is shown; optimal d_w is reached for M between 3 and 4 and is roughly proportional to $\sigma_s^{0.6\pm0.1}$.

4 Improved crucible design

Based on the trend observed in the test simulations and on practical consideration, some improvements were made to our reference parameters, see Fig. 1. First, since flux compression increases with sample radius (or when sample to crucible distance $\cong R_2 - R_s$ decreases) a relatively large sample $R_s = 15$ mm was used (actually R_1, R_2, R_c and p have been decreased, respectively to 24.5 mm, 20 mm, 31.5 mm and 11 mm, for prototype construction economy). Second, since the lift strongly depends on fluxline compression in the lower aperture (increasing as R_2/R_3), the radius R_3 was further decreased (to about 5 mm average, with some rounding), which also leaves more space for cooling channels.

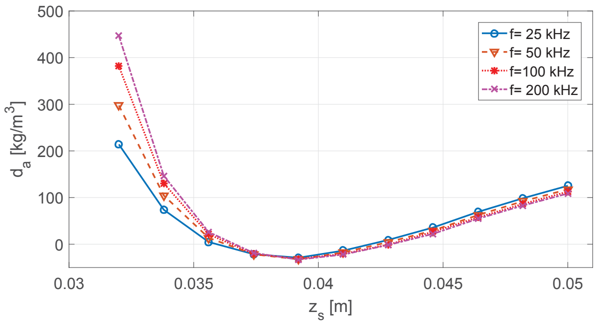

Figure 6. The critical density d_a vs sample center z_s, with $I_c = 1$ kA.

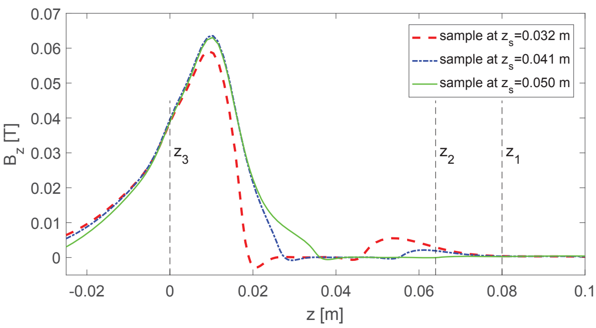

Figure 7. The field B_z along the crucible axis z for various sample position z_s, for the $f = 100$ kHz case.

New geometry considers a larger number of cuts (N_c from 10 to 12) for better uniformity, with reduced cut width $2g_s \leq 0.75$ mm, so that the leakage parameter $\mathscr{L}_c \cong 0.2$ still satisfies $\mathscr{L}_c \ll 1$. We have five or more coil turns, $N \geq 5$, and cuts are limited to $z < z_2 = 64$ mm, where now $z = z_3 = 0$ is the lower crucible face; the upper crucible face is $z = z_1 = 80$ mm. Figures 6 and 7 show the quantity of Fig. 4 for the new geometry and parameters; in particular $I_c = 1$ kA, $N_c = 10$ and $\sigma_s = 7.4 \times 10^5$ S/m; moreover $N = 6$ and coil wire radius $R_w = 4$ mm. The external boundary conditions is made with an infinite element. The magnetic field and the force obtained on the crucible has been studied as function of the sample position z_s; considering geometry constraint and large CPU-time requested for each simulation, scan of z_s was limited to the $[32, 50]$ mm interval. As manifest in Fig. 6 result for d_a, only the $z_s \in [32, 36]$ mm range is stable [that is, $d_a(z_s)$ decreasing, but positive], which is reasonable, since this range corresponds to larger d_a, achieved only when the spherical sample is very near to the crucible bottom. When the sample ball is in the middle of the crucible, lift force and d_a become zero or negative. Note also that B_z is much larger below sample than it is over sample (see fig. 7), due to the realistic absence of cuts over the $z = z_2$ planes. The maximum of magnetic field is very near to the crucible bottom. Note the perspective advantage that sample is mainly heated in its lower part, so improving convection inside sample.

This demonstrates that crucible shape can be reliably optimized even under realistic conditions, with traceable effects of design modifications. The contactless heating of alloys (in vacuum or controlled atmosphere) will allow a host of technological applications; also rf field enhancement is remarkable.

References

[1] P Jain, M Recchia, P Veltri, M Cavenago, A Maistrello and E Gaio, “Improved Methodology to Estimate the Power Transfer Efficiency in an Inductively Coupled Radio Frequency Ion Source,” *IEEE Access*, **6**, 2018, 29665, doi:10.1109/ACCESS.2018.2829618.

[2] V. Bojarevics, A. Roy and K.A. Pericleous, “Magnetic levitation of large liquid volume,” *Magnetohydrodynamics*, **46**, 2010, 339, doi:10.22364/mhd.46.4.3.

[3] M. Cavenago, T. Kulevoy and S. Petrenko, “Radio-frequency ovens for ECR ion sources,” *Rev. Sci. Instrum.*, **73**, 2002, 552.

[4] J.C. Nedelec, “Mixed Finite Elements in R^3,” *Numer. Math.*, **35**, 1980, 315.

[5] *Comsol Multiphysics 3.5* (2009) or higher version, see also http://www.comsol.eu

[6] S. Butterworth, “Effective Resistance of Inductance Coils at Radio Frequency.-Part II.,” *The Wireless Eng.*, **3**, 1926, 309.

[7] H. Nagaoka, “The Inductance Coefficient of Solenoids,” *J College Sci. Tokio*, **27**, 1909, 6.

[8] U Seydel and W Fucke, “Electrical resistivity of liquid Ti, V, Mo and W,” *J. Phys. F: Met. Phys.*, **10**, 1980, L203.